Closed-Form Expressions and Bounds for the Signal to Noise Ratio in IR-UWBoF Systems

Mohamed Shehata, *Member, IEEE*, Hassan Mostafa, *Senior Member, IEEE*, and Yehea Ismail, *Fellow, IEEE*

***Abstract*— Careful design and photonic generation of power efficient impulse radio ultra wideband (IR-UWB) waveforms by shaping their spectra is one of the most important challenges in the analysis and design of IR-UWBoF systems. Throughout this letter, theoretical expressions for the signal to noise ratio of IR-UWB waveforms in terms of their spectra are developed and optimized. Two common types of IR-UWB waveforms are considered. Numerical simulations results show excellent agreement with the obtained theoretical expressions.**

***Index Terms*— Free space path loss (FSPL), impulse radio (IR), microwave photonic (MWP), signal to noise ratio (SNR), ultra wideband over fiber (UWBoF).**

I. Introduction

WILRESS transmission of photonically generated IR-UWB waveforms is often an essential part of IR-UWBoF systems [1]. However, the limited propagation distance of UWB signals is a major challenge in UWB wireless communication systems which might prevent remote users from establishing a link with a UWB wireless access point. This is due to the severe power spectral density (PSD) constraints set by the Federal Communications Committee (FCC) [2]. Moreover, the frequency dependent channel path loss associated with the wireless transmission of IR-UWB signals tends to suppress their received PSD as well as the SNR at the electrical receiver front end. This in turn, degrades the overall system transmission performance in terms of the end-to-end bit error rate (BER). Therefore, the spectrum of an IR-UWB waveform should be carefully shaped in order to achieve the highest SNR and the minimum BER in an IR-UWB communication link. In IR-UWB systems, the SNR depends on the spectrum of the particular IR-UWB waveform that represents the transmitted symbol [3]. Most of the literature published on IR-UWB systems focus on amplitude and/or time scaled versions of the time derivatives of Gaussian [4] and sech [5] pulses. However, the frequency dependent channel path loss decreases their power spectral density (PSD) which in turn leads to a degradation in the SNR at the UWB receiver front end. In this letter, the impact of frequency dependent channel path loss on the spectra of Gaussian and sech-based IR-UWB waveforms is included. In addition, some design recommendations on how to maximize the SNR achieved by these waveforms are suggested. Throughout the rest of this letter, the derivatives of the Gaussian input basis function are denoted by the Gaussian-based IR-UWB waveforms. Similarly, waveforms obtained by differentiating a sech input basis function are denoted by sech-based IR-UWB waveforms. To the best of the authors' knowledge, there is no closed-form expressions for the SNR in terms of the PSD of these two types of IR-UWB waveforms. In this letter, an elegant approach is introduced to calculate and optimize the average SNR of these two waveform types. The developed expressions are useful in deriving closed-form expressions for the average bit error rate (BER) of various UWB modulation schemes such as on-off keying (OOK) and bi-phase modulation (BPM).

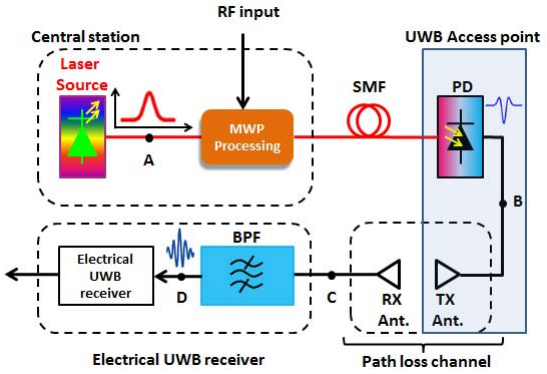

Fig. 1. Block diagram of a typical IR-UWBoF communication system. Red lines: optical paths. Black lines: electrical paths.

The rest of this letter is organized as follows. First, a typical IR-UWBoF system is described in Section (II) along with analytical expressions for the PSD of the two most common types of IR-UWB waveforms. In Section (III), theoretical expressions for the average SNR per symbol are developed in terms of the IR-UWB signal spectra and the channel model introduced in Section (II). The obtained expressions are then numerically evaluated and analyzed in Section (V). The results obtained and analyzed lead to a conclusion which is finally presented in Section (IV).

II. System Model Overview

Fig.1 depicts the block diagram of a typical IR-UWBoF system. It consists of a central station connected to a UWB access point via an optical fiber link which is followed by

Manuscript received October 27, 2016; revised January 4, 2017; accepted January 16, 2017. Date of publication January 25, 2017; date of current version March 1, 2017. This work was supported in part by Cairo University, the Zewail City of Science and Technology, in part by AUC, in part by the STDF, in part by Intel, in part by Mentor Graphics, in part by ITIDA, in part by SRC, in part by ASRT, in part by NTRA, and in part by MCIT.

M. Shehata is with the Opto Nano Electronics Laboratory, Department of Electrical Engineering, Cairo University, Giza, Egypt (e-mail: m.shehata_ieee@yahoo.com).

H. Mostafa is with the Electronics and Communications Engineering Department, Cairo University, Cairo 12613, Egypt, also with the Center of Nanoelectronics and Devices (CND) at Zewail City, 6th of October, Egypt, and also with CND, The American University in Cairo, Cairo 11835, Egypt.

Y. Ismail is with the Department of Electronics and Communications Engineering, The American University in Cairo (AUC), Cairo 11835, Egypt, and also with the Center of Nanoelectronics and Devices at Zewail City, AUC, Cairo 11835, Egypt.

Color versions of one or more of the figures in this letter are available online at http://ieeexplore.ieee.org.

Digital Object Identifier 10.1109/LPT.2017.2657750

a UWB wireless transmission link. At the central station, information in the form of a sequence of independent and identically distributed binary data symbols $d_k \in \{0, 1\}$ is applied to the RF input port of a microwave photonic (MWP) generator. A train of optical input basis functions emitted from the laser source (at point A in Fig.1) is applied to optical input of the MWP generator. The MWP generator is designed such that it shapes each optical input basis function and encodes the binary information symbols by the optically reshaped waveform. The encoded optical waveform is then propagated down a length of a dispersive fiber, usually a single mode fiber (SMF), to the UWB access point at a remote location. The optical waveform at the output of the SMF is applied to a high speed photo-detector (PD) for optical-to-electrical conversion such that the desired temporal electrical IR-UWB waveform is obtained. The electrical IR-UWB waveform is then radiated to the wireless path loss channel via the transmitter antenna and then received by the receiver antenna. The received waveform is then bandpass filtered and sent to an electrical UWB receiver for further electrical processing and detection of information symbols.

A. Common IR-UWB Waveforms

The electric field envelope of the optical pulse (at point A in Fig.1) is represented by an input basis function $\psi(t, \tau)$, where τ is its pulse shaping factor. This input basis function is given by either an amplitude normalized Gaussian pulse which is typically expressed as $\psi(t, \tau) = \exp(-t^2/{\tau_g}^2)$, $\tau_g \triangleq \tau/2\sqrt{\log(2)}$ or an amplitude normalized sech pulse which is typically expressed as $\psi(t, \tau) = \text{sech}(t/\tau_s)$, $\tau_s \triangleq \tau/2\text{sech}^{-1}(0.5)$. These definitions ensure that both the Gaussian and sech waveforms have equal full width at half maximum (FWHM) pulse widths. Throughout the analysis, it is assumed that the MWP generator applies an ideal m-th order differentiation operator to this optical envelope such that the electrical IR-UWB waveform (at point B in Fig.1) is an amplitude scaled version of a monocycle, doublet or any higher order derivative. The RF waveform at the output of the TX antenna is related to $\psi(t, \tau)$ as $\psi^{(m)}(t, \tau) = A^m d^m \psi(t, \tau)/dt^m; t \in \mathbf{R}$ where A^m is the amplitude of the IR-UWB waveform. It should be noted that A^m is adjusted such that the PSD of the IR-UWB signal does not exceed the maximum PSD admissible by the FCC mask within the useful UWB band [6]. In particular, A^m is defined as follows:

$$A^m \triangleq \left(\max\left\{S_{FCC}(\omega)\right\} / \max\left\{\left|\Psi^{(m)}(\omega, \tau)\right|^2\right\}\right)^{1/2} \quad (1)$$

where $S_{FCC}(\omega)$ is the maximum PSD admissible by the FCC mask within the useful UWB band, ω is the angular frequency, $\Psi^{(m)}(\omega, \tau) = \Im\{\psi^{(m)}(t, \tau)\}$ and $\Im\{.\}$ denotes the Fourier transform operation. The amplitude normalized Fourier transform of the m-th order Gaussian-based derivative is given by

$$\Psi^{(m)}_{n,FCC}(\omega, \tau) = A^m_g (j\omega)^m \tau_g \sqrt{\pi} \exp(-(\omega\tau_g)^2/2) \quad (2)$$

whereas the amplitude normalized Fourier transform of the m-th order sech-based derivative, $\Psi^{(m)}_{n,FCC}(\omega, \tau)$ is given by

$$\Psi^{(m)}_{n,FCC}(\omega, \tau) = A^m_s (j\omega)^m 4\pi\tau_s \text{sech}(2\pi\omega\tau_s) \quad (3)$$

In the following analysis, $\Psi^{(m)}_{n,FCC}(\omega, \tau)$ refers to one of the definitions (2) or (3) as required. Since, Gaussian and sech-based derivatives are characterized by a unique global maximum, the value of ω that leads to $\left|\Psi^{(m)}(\omega, \tau)\right|^2 = \max\left\{\left|\Psi^{(m)}(\omega, \tau)\right|^2\right\}$ is obtained by substituting either of the definitions (2) or (3) in $\partial\left|\Psi^{(m)}_{n,FCC}(\omega, \tau)\right|^2/\partial\omega = 0$ respectively and solving for ω which is defined as the peak emission angular frequency, denoted by $\omega_{p,g}$ for Gaussian-based waveforms and $\omega_{p,s}$ for sech-based waveforms. The values of A^m_g and A^m_s are obtained by substituting in $\omega_{p,g}$ and $\omega_{p,s}$ in (1) as follows.

$$A^m_g = \left(S_{FCC}(\omega)/\omega^{2m}_{p,g}\pi\tau_g^2 \exp\left(-(\omega_{p,g}\tau_g)^2/2\right)\right)^{1/2} \quad (4)$$

$$A^m_s = \left(S_{FCC}(\omega)/\omega^{2m}_{p,s}(4\pi\tau_s)^2 \text{sech}^2\left(2\pi\omega_{p,s}\tau_s\right)\right)^{1/2} \quad (5)$$

where τ_g and τ_s are the pulse widths corresponding to $\omega_{p,g}$ and $\omega_{p,s}$ respectively.

B. Arbitrary Path Loss Exponent Channel Model

The power of the received IR-UWB waveform (at point C in Fig.1) depends on the path loss of the wireless UWB channel. In general, the frequency domain transfer function of the path loss channel, measured from point B to point C in Fig.1, is modelled as [7]:

$$H_{ch}(\omega, \mathbf{r}) = \left(\frac{G_{TX}(\omega)G_{RX}(\omega)c^2}{(2\omega\|\mathbf{r}\|)^\kappa}\right)^{1/2} \exp(-j\omega\|\mathbf{r}\|/c) \quad (6)$$

where $G_{TX}(\omega)$ and $G_{RX}(\omega)$ are the frequency responses of the TX and RX antennas respectively. $\mathbf{r} \in \mathbf{R}^2$ is the position vector of the RX antenna, $\|\mathbf{r}\| \in \mathbf{R}$ is an RV which represents the physical position of the RX antenna with respect to the TX antenna, $\kappa \geq 2$ is the path loss exponent, c is the speed of light and $r_{\min}, r_{\max}$ are the minimum and the maximum TX-RX separation respectively. Let's define $\beta(\omega) \triangleq G_{TX}(\omega)G_{RX}(\omega)/(\omega)^\kappa$ and $\lambda(\mathbf{r}) \triangleq c^2/(2\|\mathbf{r}\|)^\kappa$. The dependent RV $\lambda(\mathbf{r}) : \mathbf{R}^2 \rightarrow \mathbf{R}$ represents the large scale channel path loss at different positions of the RX antenna. The particular value of κ depends on the specific environment in which the TX and RX antennas are immersed. The frequency response of the TX and RX antennas depends on the particular design of each antenna. For simplicity and without loss of generality, both antennas are assumed to have a flat frequency response at least over the useful UWB band. Therefore, the frequency dependence of both $G_{TX}(\omega)$ and $G_{RX}(\omega)$ are dropped throughout the rest of the analysis. Moreover, both the TX and RX antennas are assumed to have omni-directional radiation characteristics such that the receivers surrounding the TX antenna can access the IR-UWB signal equally likely.

III. Signal to Noise Ratio Analysis

At the receiver input, the spectrum of the received IR-UWB waveform may not be fully compliant to the FCC spectral constraints and is corrupted by a zero mean AWGN random process with a double sided PSD of N_o. Therefore, the PSD of the received signal is passed to an ideal bandpass filter (BPF) in order to extract the signal power in the useful UWB band while reducing the out-of-band AWGN power. This BPF is assumed to have an ideally flat frequency response,

at least over the useful UWB band, lower and upper cutoff angular frequencies of ω_L and ω_H respectively and an angular passband of $\Omega = \omega_H - \omega_L$. The frequency domain transfer function of the BPF is given by

$$H_{BPF}(\omega) = \begin{cases} 1; & \omega_L \leq \omega \leq \omega_H \\ 0; & \text{elsewhere} \end{cases} \tag{7}$$

After bandpass filtering, the received signal becomes strictly fully compliant with the FCC spectral constraints. The received signal spectrum (at point D in Fig.1) is given by

$$\Upsilon(\omega) = \begin{cases} H_{ch}(\omega, \mathbf{r})\Psi^{(m)}_{n,FCC}(\omega, \tau)H_{BPF}(\omega); & \omega \in [\omega_H, \omega_L] \\ 0; & \text{elsewhere} \end{cases} \tag{8}$$

The total effective noise power becomes $N_o\Omega/\pi$. The SNR at the receiver side can be expressed as follows:

$$\begin{aligned} \mathbf{SNR}_{RX}(\tau|\mathbf{r}) &= \frac{\pi}{N_o\Omega}\int_{-\infty}^{\infty}\left|\lambda(\mathbf{r})\beta(\omega)\Psi^{(m)}_{n,FCC}(\omega,\tau)\right|^2 d\omega \\ &= \frac{2\pi\lambda}{N_o\Omega}\int_{\omega_L}^{\omega_H}\omega^{\overline{m}}\left|\Psi^{(m)}_{n,FCC}(\omega,\tau)\right|^2 d\omega \end{aligned} \tag{9}$$

where $\overline{m} = 2m - \kappa$. The SNR in (9) is implicitly conditional to the receiver's location. The corresponding average SNR can be obtained by averaging (9) over the probability density function (PDF) of λ. Thus, the average SNR is given by

$$\begin{aligned} \overline{\mathbf{SNR}}_{RX}(\tau) &= \mathbf{E}\left\{\frac{2\pi\lambda}{N_o\Omega}\int_{\omega_L}^{\omega_H}\omega^{-\kappa}\left|\Psi^{(m)}_{n,FCC}(\omega,\tau)\right|^2 d\omega\right\} \\ &= \frac{2\pi}{N_o\Omega}\int_0^{\infty}\int_{\omega_L}^{\omega_H}\lambda\omega^{-\kappa}\left|\Psi^{(m)}_{n,FCC}(\omega,\tau)\right|^2 P(\lambda)d\omega d\lambda \\ &= \frac{2\pi\,\bar{\lambda}}{N_o\Omega}\int_{\omega_L}^{\omega_H}\omega^{-\kappa}\left|\Psi^{(m)}_{n,FCC}(\omega,\tau)\right|^2 d\omega \end{aligned} \tag{10}$$

where $\mathbf{E}\{.\}$ denotes the expectation operator, $\bar{\lambda} = \mathbf{E}\{\lambda\} = \int_0^{\infty}\lambda P(\lambda)d\lambda$ and $P(\lambda)$ is the PDF of λ. As mentioned before in Section (II), the RX is equally likely to be found at a distance $\|\mathbf{r}\|$ from the TX. Therefore, it is reasonable to assume a uniform PDF $P_{\mathbf{r}}(\|\mathbf{r}\|)$ for $\|\mathbf{r}\|$ as follows:

$$P_{\mathbf{r}}(\|\mathbf{r}\|) = \begin{cases} \dfrac{1}{\pi(r^2_{\min} - r^2_{\max})}; & r_{\min} \leq \|\mathbf{r}\| \leq r_{\max} \\ 0; & \text{elsewhere} \end{cases} \tag{11}$$

Consequently, $\overline{\lambda}$ is given by the κ^{th} moment of the inverse uniform distribution of $\|\mathbf{r}\|$ and the average channel path loss can be expressed as follows.

$$\mathbf{E}\{\lambda\} = \frac{G_{TX}G_{RX}c^2}{(2\pi)^{\kappa}(\kappa-1)}\frac{r^{2-2\kappa}_{\min} - r^{2-2\kappa}_{\max}}{r^2_{\max} - r^2_{\min}} \tag{12}$$

Now let's evaluate the integral in (10). For Gaussian-based IR-UWB waveforms, substituting (2) in (10) yields:

$$\begin{aligned} \overline{\mathbf{SNR}}_{RX}(\tau) &= \frac{\bar{\lambda}\,(\pi\tau_g A^m_g)^2}{N_o\Omega}\int_{\omega_L}^{\omega_H}\omega^{\bar{m}}\exp\left(-(\omega\tau_g)^2\right)d\omega \\ &= \frac{\bar{\lambda}\,(\pi\tau_g A^m_g)^2}{N_o\Omega}\left(\frac{\sqrt{2}}{\tau_g}\right)^{\bar{m}+1} \\ &\quad\times\left(\Xi(\omega_H\tau_g/\sqrt{2}) - \Xi(\omega_L\tau_g/\sqrt{2})\right) \end{aligned} \tag{13}$$

where

$$\begin{aligned} \Xi(u) &= (1-s)\Gamma\left(\frac{\bar{m}+s+1}{2}\right)erf(u) - \exp(-u^2) \\ &\quad\times\sum_{n=0}^{L-1}\frac{\Gamma(\frac{\bar{m}+1}{2})u^{\bar{m}-2n-1}}{\Gamma(\frac{\bar{m}+1}{2}-n)}, \end{aligned}$$

$\Gamma(.)$ is the gamma function defined as $\Gamma(z) = \int_{y=0}^{\infty} y^{z-1}\exp(-y)dy$, $erf(u) = (2/\sqrt{\pi})\int_0^u \exp(-y^2)dy$ is the Gaussian error function, $L = (\bar{m}+s)/2$, $s = 0$ if $\overline{m}$ is odd and $s = 1$ if $\overline{m}$ is even. Likewise, the integral in (10) is also evaluated for sech-based IR-UWB waveforms by substituting (3) in (10) as follows:

$$\begin{aligned} \overline{\mathbf{SNR}}_{RX}(\tau) &= \frac{2\pi\,\bar{\lambda}\left(A^m_s\right)^2}{N_o\Omega}\int_{\omega_L}^{\omega_H}\omega^{\bar{m}}(4\pi\tau_s)^2\mathrm{sech}^2(2\pi\omega\tau_s)d\omega \\ &= \frac{8\pi\,\bar{\lambda}\,\bar{m}!(4\pi\tau_s A^m_s)^2}{N_o\Omega}\left(\frac{1}{2\pi\tau_s}\right)^{\bar{m}+1} \\ &\quad\times(\Lambda(2\pi\omega_H\tau_s) - \Lambda(2\pi\omega_L\tau_s)) \end{aligned} \tag{14}$$

where

$$\Lambda(\mathrm{u}) = \sum_{l=0}^{K}\sum_{q=0}^{\bar{m}}\frac{(-1)^{l+q}(l+1)}{(\bar{m}-q)!(-2(l+1))^{q+1}}u^{\bar{m}-q}\exp(-2(l+1)u)$$

and $K \gg 1$. The larger is K, the more accurate will be $\Lambda(\mathrm{u})$. The integrals in (13) and (14) can also be evaluated by using numerical integration techniques as shall be clear in the following section.

IV. Simulation Results and SNR Otimization: Optimal Pulse Widths

In this section, the average SNR expressions in (13) and (14) are numerically evaluated and optimized with respect to τ. The integrals in (13) and (14) are numerically evaluated by using the trapezoidal rule in order to confirm the validity of their closed form equivalents. The noise power is evaluated by using Monte Carlo numerical simulation technique. A number of 10^3 sample realization AWGN noise vectors $\mathbf{n} \in \mathbf{C}^{1\times N}$ having a variance of $N_o\Omega$ and a sample size of $N = 10^3$ are generated. The noise power is then calculated by averaging $\mathbf{n}\mathbf{n}^H$ over these realizations, where $(.)^H$ is the Hermitian operator. The path loss exponent $\kappa = 2$. The values of $r_{\min}$ and $r_{\max}$ are 4 m and 10 m respectively. Accordingly, the average FSPL channel loss is -75 dB. The FWHM pulse width τ is varied from 0 to 500 ps for Gaussian-based IR-UWB waveforms

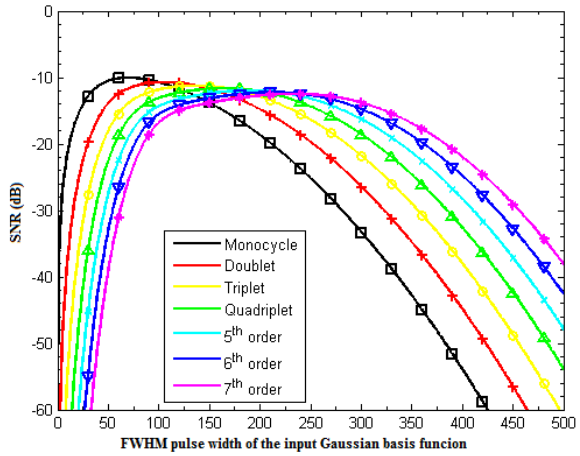

Fig. 2. Average SNR versus the FWHM pulse width of the Gaussian input basis function. Solid lines: theoretically obtained results. Markers: Results obtained by numerical integration techniques.

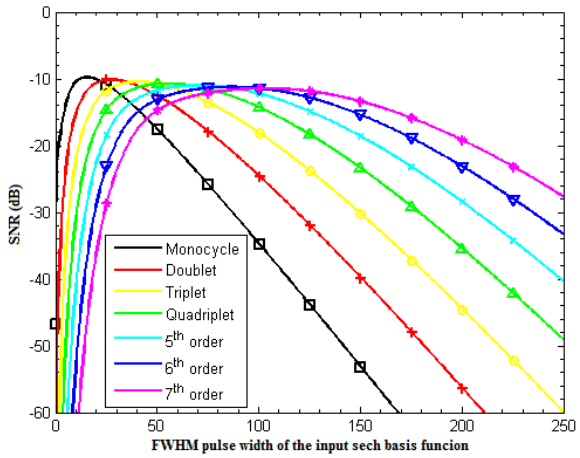

Fig. 3. Average SNR versus the FWHM pulse width of the sech input basis function. Solid lines: theoretically obtained results. Markers: Results obtained by numerical integration techniques.

and from 0 up to 250 ps for sech-based IR-UWB waveforms. The derivative order m takes the values through $\{1, 2, ...7\}$. According to [2], f_L = 3.1 GHz, f_H = 10.6 GHz and $\max\{S_{FCC}(\omega)\}$ = -41.3 dBm/MHz. The noise PSD $N_o = k_B T_o$, where $k_B = 1.23 \times 10^{-38}$ J/K is the Boltzmann constant and To=300 K is the nominal receiver noise temperature. The simulation starts by evaluating the values of $(\tau_g, A_g^m, \omega_{p,g})$ and $(\tau_s, A_s^m, \omega_{p,s})$ numerically. Based on the derived expression in (13) and (14), Figs. 2 and 3 show the average SNR versus τ at different values of m for Gaussian-based and sech-based IR-UWB waveforms respectively.

Both figures indicate that, at a particular value of m, the average SNR of Gaussian-based and sech-based IR-UWB waveforms increases monotonically toward a maximum value with increasing τ from zero up to an optimum value where the average SNR attains its maximum. For example, in Fig.2, a Gaussian-based monocycle pulse having a FWHM pulse width of 68.84 ps achieves the maximum average SNR of -10.03 dB. Similarly, in Fig.3, the sech-based monocycle pulse achieves a maximum SNR value of -9.76 dB at a FWHM input pulse width of 15.36 ps.

It is important to note that, the sech-based monocycle outperforms its Gaussian-based counterpart in terms of the maximum achievable average SNR at a much lower pulse width. This is true for any pair of Gaussian and sech-based waveform types of the same order m. Furthermore, increasing τ beyond its optimum value leads to a degradation of the average SNR below its maximum value regardless of the waveform type and the particular value of m, (i.e. Gaussian-based and sech-based doublets, triplets and higher order derivatives also show similar behavior). On the other hand, the maximum attainable average SNR decreases with increasing m. This is because increasing the differentiation order m leads to shifting the UWB signal spectrum towards higher frequencies outside the window of the useful UWB band. Correspondingly, less power is produced at the output of the BPF within this band.

Moreover, it is important to highlight that an m-th order Gaussian-based waveform outperforms all waveforms of order $n < m$ when $\tau < 100$ ps. However, for $\tau < 250$ ps, the situation is reversed and the superiority of lower order derivatives emerges. In this case, an n-th order Gaussian-based waveform achieves a SNR higher than that achieved by a waveforms of order $m>n$. For pulse widths between 100 ps and 250 ps, the superiority of one waveform over another is determined by its particular width and order. For sech-based IR-UWB waveforms, the low pulse width regime ranges from 0 to about 21 ps, while the high pulse width regime starts from about 100 ps. For pulse widths between 21 ps and 100 ps, the superiority of one waveform over another is determined by its particular width and order. All of the above observations reveal that sech-based IR-UWB waveforms are preferred over their Gaussian-based counterparts as the former support information transmission at higher data rates and SNRs.

V. Conclusion

This letter presents an analytical method to maximize the received electrical SNR of IR-UWB waveforms subject to the FCC spectral constraints. Closed form expressions for the average SNR are derived. It is also shown that for each waveform type, the SNR can be maximized by tuning the pulse width of these waveforms. The applicability of the obtained SNR expressions in obtaining closed form BER expressions for different modulation schemes is an open research point that needs a lot of further investigation.

References

[1] R. R. Lopez, A. Caballero, X. Yu, T. B. Gibbon, J. B. Jensen, and I. T. Monroy, "A comparison of electrical and photonic pulse generation for IR-UWB on fiber links," *IEEE Photon. Technol. Lett.*, vol. 22, no. 5, pp. 263–265, Mar. 1, 2010.

[2] U.S. Federal Communications Commission, "Revision of part 15 of the commission's rules regarding ultra-wideband transmission systems," U.S. Federal Commun. Commission, Washington, DC, USA, Tech. Rep. FCC 02-48, Apr. 2002.

[3] M. Ghavami, L. B. Michael, and R. Kohno, *Ultra Wideband Signals and Systems in Communication Engineering*, 2nd ed. West Sussex, U.K.: Wiley, 2007.

[4] Q. Wang and J. Yao, "Ultra-wideband Gaussian monocycle and doublet pulse generation using a reconfigurable photonic microwave delay-line filter," in *Proc. IEEE Radio Wireless Symp.*, Jan. 2008, pp. 129–132.

[5] C. Wang, F. Zeng, and J. Yao, "All-fiber ultrawideband pulse generation based on spectral shaping and dispersion-induced frequency-to-time conversion," *IEEE Photon. Technol. Lett.*, vol. 19, no. 3, pp. 137–139, Feb. 1, 2007.

[6] M. Abtahi, M. Mirshafiei, S. LaRochelle, and L. A. Rusch, "All-optical 500-Mb/s UWB transceiver: An experimental demonstration," *J. Lightw. Technol.*, vol. 26, no. 15, pp. 2795–2802, Aug. 1, 2008.

[7] T. Wang, W. Heinzelman, and A. Seyedi, "Link energy minimization in IR-UWB based wireless networks," *IEEE Trans. Wireless Commun.*, vol. 9, no. 9, pp. 2800–2811, Sep. 2010.